ATOMIC NORM DENOISING FOR MULTI-FREQUENCY-SNAPSHOT DOA ESTIMATION

Yongsung Park[⋆] *Peter Gerstoft*[⋆] *Yifan Wu*[⋆] *Michael B. Wakin*[†]

[⋆] NoiseLab, University of California San Diego, La Jolla, CA, USA
[†] Colorado School of Mines, Golden, CO, USA

2024 IEEE 13th Sensor Array and Multichannel Signal Processing Workshop (SAM) | 979-8-3503-4481-3/24/$31.00 ©2024 IEEE | DOI: 10.1109/SAM60225.2024.10636678

ABSTRACT

Motivated by atomic norms in gridless sparse signal recovery, we introduce a gridless direction-of-arrival (DOA) estimator capable of handling scenarios with multiple frequencies and multiple snapshots. Within the atomic norm framework, we consider a multi-frequency model analogous to a multi-snapshot model. Subsequently, we extend the model to accommodate both multi-snapshot and multi-frequency data. The proposed method is illustrated through numerical simulations and validated using ocean acoustic experimental data.

Index Terms— DOA estimation, atomic norm minimization, multi-frequency model, multiple measurement vectors

1. INTRODUCTION

Atomic norm minimization (ANM) [1–8] enables gridless sparse plane-wave direction-of-arrival (DOA) estimation using linear arrays. Sparse processing provides high-resolution DOA estimation, while gridless processing avoids DOA bias caused by grid mismatch [9–13]. More accurate estimation can be achieved when diverse observations are available. Multiple measurement vectors (MMVs) offer one type of diversity through multiple temporal snapshots. Another type of diversity comes from sources with multiple temporal frequencies. We propose a gridless sparse DOA estimator that can handle such multi-snapshot and multi-frequency data.

Sparse regularization, as used in compressive sensing (CS), promotes sparse solutions, resulting in sharp peak beamforming spectra and enhanced high-resolution DOA estimation [14–16]. A challenge in sparse DOA methods lies in the mismatch between the angular grid and actual DOAs [1, 2, 17]. To address this, a gridless sparse processing method has been introduced and applied to DOA estimation. For an overview of sparse DOA estimation, see [1–3, 6].

ANM enables gridless sparse DOA estimation. Consider when multiple time snapshots are available and the data share a common sparsity profile across snapshots (i.e., the DOAs are consistent across time) [14, 16]. This enables ANM with MMV to achieve multi-snapshot gridless sparse DOA estimation [11, 13, 18–20].

This work is supported by NSF Grant CCF-1704204, NSF Grant CCF-2203060, and Office of Naval Research (ONR) Grant N00014-21-1-2267.

Steering vectors (or array manifold vectors) in plane-wave DOA estimation are frequency-dependent, making it challenging to process multi-frequency data in a similar way to multi-snapshot processing. It may be possible to estimate DOAs for each frequency and then determine final DOA estimates based on the obtained DOA estimates across frequencies. However, this method could offer less processing gain compared to joint processing of multi-frequency data.

Our contributions are as follows:

1) We propose an ANM-based DOA estimator capable of handling multi-snapshot and multi-frequency data. Our model addresses multiple frequencies jointly. [21–26] utilized certain properties of steering vectors for multi-frequency processing, enabling approaches similar to multi-snapshot processing. We utilize the *nominal frequency-virtual array element spacing* concept for our multi-frequency processing. This concept facilitates the formation of a common sparsity profile for the data across frequencies. Similar to multi-snapshot processing, we align and process multiple frequency data.

2) The model [24, 25] is a multi-frequency model with a single snapshot. In contrast, our proposed model handles multiple snapshots. Within the ANM framework, [25] adopts the dual problem of ANM and the dual semidefinite programming (SDP). An extension [27] deals with non-uniform arrays, non-uniform frequency spacing, and multiple snapshots, following a regularization-free primal domain SDP with root MUSIC for enhanced robustness. Our work adopts atomic norm denoising with atomic norm soft thresholding (AST) and its SDP [19, 28]. The model is an AST-based method for handling MMV, including multiple snapshots and multiple frequencies.

3) The proposed technique is applied to ocean acoustic experimental data.

2. ARRAY DATA MODEL

Consider K DOAs with L snapshots at frequencies f_i, $i = 1, \ldots, F$. We assume the sources with DOAs $\theta_k \in [-90°, 90°)$ are in the far-field of a uniform linear array (ULA) with M sensors. Let $\mathbf{X}_{f_i} \in \mathbb{C}^{K \times L}$ be the source amplitudes; for the kth DOA at time t_l, $[\mathbf{X}_{f_i}]_{k,t_l} \in \mathbb{C}$, $k = 1, \ldots, K$, $l = 1, \ldots, L$.

The array data $\mathbf{Y}_{f_i} = [\mathbf{y}_{t_1,f_i} \dots \mathbf{y}_{t_L,f_i}] \in \mathbb{C}^{M\times L}$ is

$$\mathbf{Y}_{f_i} = \sum_{k=1}^{K} \mathbf{a}_{f_i}(\theta_k)[\mathbf{X}_{f_i}]_{k,:}^{\mathsf{T}} + \mathbf{E}_{f_i}, \tag{1}$$

where $[\mathbf{X}_{f_i}]_{k,:} = \big[[\mathbf{X}_{f_i}]_{k,t_1} \dots [\mathbf{X}_{f_i}]_{k,t_L}\big] \in \mathbb{C}^L$, $\mathbf{E}_{f_i} \in \mathbb{C}^{M\times L}$ is the additive noise, and the steering vector

$$\mathbf{a}_{f_i}(\theta) = \big[e^{-j\frac{2\pi f_i}{c}0\cdot d\sin\theta} \dots e^{-j\frac{2\pi f_i}{c}(M-1)\cdot d\sin\theta}\big]^{\mathsf{T}} \in \mathbb{C}^M, \tag{2}$$

where c is the propagation speed and d is the ULA element spacing. The additive noise $\mathbf{E}_{f_i}$ is assumed independent across sensors, snapshots, and frequencies, with each element following a complex Gaussian $\mathcal{CN}(0,\sigma^2)$. The signal-to-noise ratio (SNR) for a single snapshot is used, defined as $\text{SNR} = 20\log_{10}\big(\big\|\sum_{k=1}^{K}[\mathbf{X}_{f_i}]_{k,t_l}\mathbf{a}_{f_i}(\theta_k)\big\|_2 / \big\|[\mathbf{E}_{f_i}]_{:,t_l}\big\|_2\big)$.

3. ANM DOA ESTIMATION WITH MMV

This section gives a review of gridless sparse DOA estimation using ANM [1–3, 6, 10] for MMV following [9, 11].

The noiseless, single frequency f data with K DOAs (1) having L snapshots, $\mathbf{Y}_f^\star \in \mathbb{C}^{M\times L}$, is,

$$\mathbf{Y}_f^\star = \sum_{k=1}^{K} \mathbf{a}_f(\theta_k)[\mathbf{X}_f]_{k,:}^{\mathsf{T}}. \tag{3}$$

The atom and atomic set for gridless sparse DOA estimation are defined as $\mathbf{\Psi}(\theta_k, \boldsymbol{\phi}_{k:}) = \mathbf{a}_f(\theta_k)\boldsymbol{\phi}_{k:}^{\mathsf{T}}$ with $\theta_k \in [-90^\circ, 90^\circ)$, $\boldsymbol{\phi}_{k:} \in \mathbb{C}^L$, $\|\boldsymbol{\phi}_{k:}\|_2 = 1$, and $\mathcal{A} = \{\mathbf{\Psi}(\theta_k, \boldsymbol{\phi}_{k:}) : \theta_k \in [-90^\circ, 90^\circ), \|\boldsymbol{\phi}_{k:}\|_2 = 1\}$. The atomic norm of the noise-free data $\mathbf{Y}_f^\star$ (3) is defined as [1, 28]

$$\big\|\mathbf{Y}_f^\star\big\|_{\mathcal{A}} = \inf_{\substack{\xi_k \geq 0,\\ \theta_k, \boldsymbol{\phi}_{k:}}} \left\{ \sum_{k=1}^{K} \xi_k : \mathbf{Y}_f^\star = \sum_{k=1}^{K} \xi_k \mathbf{a}_f(\theta_k)\boldsymbol{\phi}_{k:}^{\mathsf{T}} \right\}. \tag{4}$$

The atomic norm (4) is equivalent to the solution of the following semidefinite program (SDP) [1, (II.6)],

$$\begin{aligned} \big\|\mathbf{Y}_f^\star\big\|_{\mathcal{A}} = \min_{\mathbf{u},\mathbf{V}_L} \ & \frac{1}{2M}\text{Tr}\big(\text{Toep}(\mathbf{u})\big) + \frac{1}{2}\text{Tr}(\mathbf{V}_L) \\ \text{s.t.} \ & \begin{bmatrix} \text{Toep}(\mathbf{u}) & \mathbf{Y}_f^\star \\ \mathbf{Y}_f^{\star\mathsf{H}} & \mathbf{V}_L \end{bmatrix} \succeq 0, \end{aligned} \tag{5}$$

where $\mathbf{V}_L \in \mathbb{C}^{L\times L}$ is a free matrix variable.

With noisy data $\mathbf{Y}_f$ (1), we solve (5) in the regularized optimization problem as the LASSO [14, 29]-like way, referred to as AST [19, 28],

$$\min_{\mathbf{Y}_f^\star} \frac{1}{2}\|\mathbf{Y}_f - \mathbf{Y}_f^\star\|_{\mathsf{F}}^2 + \tau\|\mathbf{Y}_f^\star\|_{\mathcal{A}}. \tag{6}$$

The regularization parameter τ balances the sparsity level in $\mathbf{Y}_f^\star$ and the data fitting $(\mathbf{Y}_f - \mathbf{Y}_f^\star)$, and is empirically chosen.

Using the equivalent SDP formulation (5), the SDP formulation of (6) is given by [28, Eq. (19)], [19, Eq. (12)]

$$\begin{aligned} \min_{\substack{\mathbf{Y}_f^\star,\\ \mathbf{u},\mathbf{V}_L}} \ & \frac{1}{2}\|\mathbf{Y}_f - \mathbf{Y}_f^\star\|_{\mathsf{F}}^2 + \frac{\tau}{2}\Big(\frac{1}{M}\text{Tr}\big(\text{Toep}(\mathbf{u})\big) + \text{Tr}(\mathbf{V}_L)\Big) \\ \text{s.t.} \ & \begin{bmatrix} \text{Toep}(\mathbf{u}) & \mathbf{Y}_f^\star \\ \mathbf{Y}_f^{\star\mathsf{H}} & \mathbf{V}_L \end{bmatrix} \succeq 0. \end{aligned} \tag{7}$$

The CVX program [30] can solve (7). The primal solution $\mathbf{Y}_f^\star$ and the dual solution $\mathbf{Q} \in \mathbb{C}^{M\times L}$ are specified by the optimality conditions. There is no duality gap [1, 28]: (i) $\mathbf{Y}_f = \mathbf{Y}_f^\star + \mathbf{Q}$, (ii) $\|\mathbf{Q}\|_{\mathcal{A}*} \leq \tau$, and (iii) $\langle \mathbf{Q}, \mathbf{Y}_f^\star \rangle_{\mathbb{R}} = \tau\|\mathbf{Y}_f^\star\|_{\mathcal{A}}$.

To retrieve DOAs, ANM obtains the DOAs using $\mathbf{Y}_f^\star$ (7) and $\mathbf{Q} = \mathbf{Y}_f - \mathbf{Y}_f^\star$, by locating those points where

$$\mathcal{Q}(\theta) = \|\mathbf{Q}^{\mathsf{H}}\mathbf{a}_f(\theta)\|_2^2 = \tau^2. \tag{8}$$

4. ANM WITH MULTIPLE FREQUENCIES

We simultaneously process multi-frequency data within the ANM framework. A multi-frequency model is formulated similar to a multi-snapshot model. The nominal frequency-virtual array element spacing allows the data to share a common sparsity profile, similar to multi-snapshot models. We align multi-frequency data and then expand the model to encompass both multi-frequency and multi-snapshot data.

Multi-frequency processing considers multiple frequencies jointly. For simplicity of notation, here we specialize the multi-frequency processing to $F = 2$ frequencies $\{f_1, f_2\}$. For a true DOA θ, the phase angle of the $m+1$th element of the steering vectors $\{\mathbf{a}_{f_1}, \mathbf{a}_{f_2}\}$ are given by

$$\begin{aligned} \angle\mathbf{a}_{f_1}(\theta, d) &= -\frac{2\pi}{c}f_1 dm\sin\theta = -\frac{2\pi}{c}\frac{f_1}{\mu'}(\mu' d)m\sin\theta \\ &= \angle\mathbf{a}_{f_\mathcal{N}}(\theta, \mu' d), \end{aligned} \tag{9}$$

$$\begin{aligned} \angle\mathbf{a}_{f_2}(\theta, d) &= -\frac{2\pi}{c}f_2 dm\sin\theta = -\frac{2\pi}{c}\frac{f_1}{\mu'}(\mu'' d)m\sin\theta \\ &= \angle\mathbf{a}_{f_\mathcal{N}}(\theta, \mu'' d), \end{aligned} \tag{10}$$

where the nominal frequency $f_\mathcal{N} = f_1/\mu'$ and $\mu', \mu'' \in \mathbb{Z}$ are integers for simplifying f_2/f_1 using cross-cancelling, i.e., $\mu'/\mu'' = f_1/f_2$. Note that, the steering vectors $\{\mathbf{a}_{f_1}, \mathbf{a}_{f_2}\}$ share the same nominal frequency $f_\mathcal{N}$ but with different element virtual spacing $\{\mu' d, \mu'' d\}$.

In Fig. 1, we illustrate the multi-snapshot-frequency modeling with $F = 4$ frequencies, $f_i \in \{f_1, 1.5f_1, 2f_1, 2.5f_1\}$ and element spacing d. Based on the nominal frequency $f_\mathcal{N} = f_1/2$ ($\mu' = 2$), multiple frequency samples are reexpressed to have $f_\mathcal{N}$ with element spacing $\{2d, 3d, 4d, 5d\}$ ($\mu'' = 2, 3, 4, 5$).

The mth element of $\mathbf{y}_{t_l,f_i} \in \mathbb{C}^M$ is mapped into the virtual spacing, i.e. [25], (see Fig. 1),

$$\big[\widetilde{\mathbf{y}}_{t_l,f_i}\big][(f_i/f_\mathcal{N})(m-1)+1] = \big[\mathbf{y}_{t_l,f_i}\big][m], \tag{11}$$

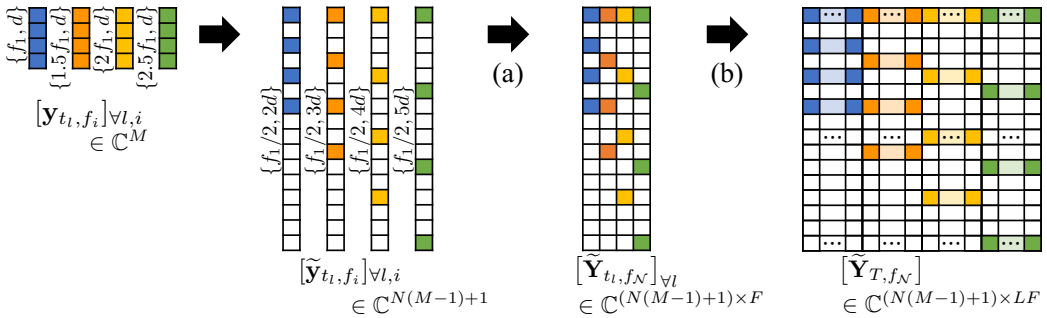

Fig. 1: Multi-snapshot-frequency model. (a) Multi-frequency-data ($f_i \in \{f_1, 1.5f_1, 2f_1, 2.5f_1\}$, $F=4$) are transformed with the nominal frequency $f_\mathcal{N} = f_1/2$ and grouped. (b) Multi-frequency processing (F-MMV) is extended to multi-snapshot-frequency processing (LF-MMV).

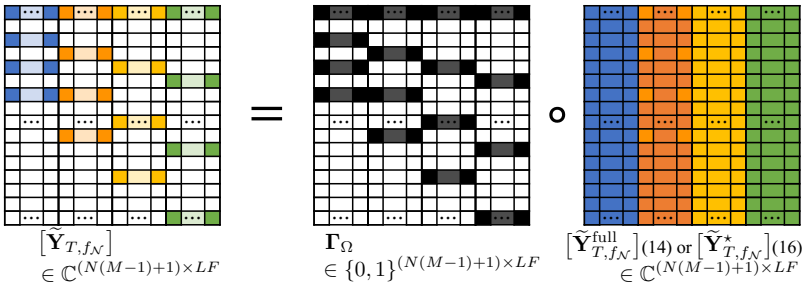

Fig. 2: Multi-snapshot-frequency [Sec. 4] as a sparse linear array model and the element-selection $\mathbf{\Gamma}_\Omega$, see (14) and (16).

where $[\widetilde{\mathbf{y}}_{t_l,f_i}] \in \mathbb{C}^{N(M-1)+1}$ with $N = f_F/f_\mathcal{N}$ (f_F is the largest frequency).

Multiple frequency samples at a single time t_l, $[\widetilde{\mathbf{y}}_{t_l,f_i}]$ (11), $i=1,\ldots,F$, share the same nominal frequency $f_\mathcal{N} = f_1/\mu'$. We group them into a matrix

$$\widetilde{\mathbf{Y}}_{t_l,f_\mathcal{N}} = \big[\widetilde{\mathbf{y}}_{t_l,f_1} \ldots \widetilde{\mathbf{y}}_{t_l,f_F}\big] \in \mathbb{C}^{(N(M-1)+1)\times F}. \tag{12}$$

For multi-snapshot processing, the single snapshot multi-frequency data $\widetilde{\mathbf{Y}}_{t_l,f_\mathcal{N}}$, $l=1,\ldots,L$, is extended to a matrix

$$\begin{aligned}\widetilde{\mathbf{Y}}_{T,f_\mathcal{N}} &= \big[\widetilde{\mathbf{y}}_{t_1,f_1} \ldots \widetilde{\mathbf{y}}_{t_L,f_1} \ldots \widetilde{\mathbf{y}}_{t_1,f_F} \ldots \widetilde{\mathbf{y}}_{t_L,f_F}\big] \\ &\in \mathbb{C}^{(N(M-1)+1)\times LF}.\end{aligned} \tag{13}$$

Suppose data $\widetilde{\mathbf{Y}}^{\text{full}}_{T,f_\mathcal{N}} \in \mathbb{C}^{(N(M-1)+1)\times LF}$, which are full ULA data with $N(M-1)+1$ sensors with the element spacing d, observe sources having the same DOAs θ_k and amplitudes $[\mathbf{X}_{f_i}]_{k,t_l} \in \mathbb{C}$, $i=1,\ldots,F$, $k=1,\ldots,K$, and $l=1,\ldots,L$ as in (1), i.e.,

$$\widetilde{\mathbf{Y}}^{\text{full}}_{T,f_\mathcal{N}} = \big[\widetilde{\mathbf{y}}^{\text{full}}_{t_1,f_1} \ldots \widetilde{\mathbf{y}}^{\text{full}}_{t_L,f_1} \ldots \widetilde{\mathbf{y}}^{\text{full}}_{t_1,f_F} \ldots \widetilde{\mathbf{y}}^{\text{full}}_{t_L,f_F}\big], \tag{14a}$$

$$\widetilde{\mathbf{y}}^{\text{full}}_{t_l,f_i} = \sum_{k=1}^{K} \mathbf{a}^{\text{full}}_{f_\mathcal{N}}(\theta_k)[\mathbf{X}_{f_i}]^{\mathsf{T}}_{k,t_l} + \mathbf{E}^{\text{full}}_{f_i}, \tag{14b}$$

$$\big[\mathbf{a}^{\text{full}}_{f_\mathcal{N}}(\theta)\big][m'] = e^{-j\frac{2\pi f_\mathcal{N}}{c}(m'-1)\cdot d\sin\theta}, \tag{14c}$$

where $m'=1,\ldots,N(M-1)+1$. The data $\widetilde{\mathbf{Y}}_{T,f_\mathcal{N}}$ (13) is a subset of $\widetilde{\mathbf{Y}}^{\text{full}}_{T,f_\mathcal{N}}$ (14), i.e.,

$$\widetilde{\mathbf{Y}}_{T,f_\mathcal{N}} = \mathbf{\Gamma}_\Omega \circ \widetilde{\mathbf{Y}}^{\text{full}}_{T,f_\mathcal{N}}, \tag{15}$$

where $\mathbf{\Gamma}_\Omega \in \{0,1\}^{(N(M-1)+1)\times LF}$ is the element-selection matrix having all 0 but 1 at the non-zero positions in $\widetilde{\mathbf{Y}}_{T,f_\mathcal{N}}$ (13) and "$\circ$" denotes the Hadamard product, see Fig. 2.

Multi-frequency processing transforms frequencies to one nominal frequency and aligns and processes multi-frequency-data jointly as in (12). Multi-snapshot-frequency processing groups all multi-snapshot and multi-frequency data as in (13). Using (7) and (13), we have the optimization problem for multi-snapshot-frequency processing as the follows,

$$\begin{aligned}\min_{\substack{\widetilde{\mathbf{Y}}^{\star}_{T,f_\mathcal{N}},\\ \mathbf{u},\mathbf{V}_L}} \ & \frac{1}{2}\|\widetilde{\mathbf{Y}}_{T,f_\mathcal{N}} - \mathbf{\Gamma}_\Omega \circ \widetilde{\mathbf{Y}}^{\star}_{T,f_\mathcal{N}}\|^2_{\mathsf{F}} + \frac{\tau}{2}\Big(\frac{1}{M}\mathrm{Tr}\big(\mathrm{Toep}(\mathbf{u})\big) + \mathrm{Tr}(\mathbf{V}_L)\Big) \\ \text{s.t.} \ & \begin{bmatrix} \mathrm{Toep}(\mathbf{u}) & \widetilde{\mathbf{Y}}^{\star}_{T,f_\mathcal{N}} \\ \widetilde{\mathbf{Y}}^{\star\mathsf{H}}_{T,f_\mathcal{N}} & \mathbf{V}_L \end{bmatrix} \succeq 0.\end{aligned} \tag{16}$$

As in (8), the DOAs are where

$$\mathcal{Q}(\theta) = \|\widetilde{\mathbf{Q}}^{\mathsf{H}}\mathbf{a}^{\text{full}}_{f_\mathcal{N}}(\theta)\|^2_2 = \tau^2, \tag{17a}$$

$$\widetilde{\mathbf{Q}} = \widetilde{\mathbf{Y}}_{T,f_\mathcal{N}} - \mathbf{\Gamma}_\Omega \circ \widetilde{\mathbf{Y}}^{\star}_{T,f_\mathcal{N}}. \tag{17b}$$

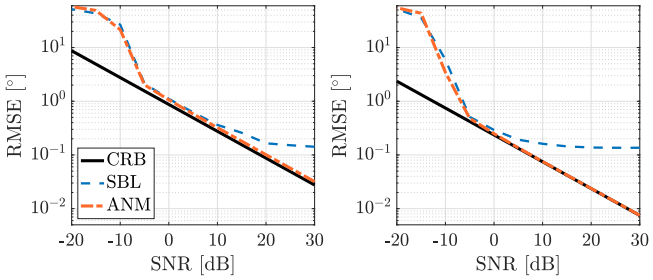

(a) 1 DOA, $F=1$ (b) 1 DOA, $F=4$

(c) 3 DOAs, $F=1$ (d) 3 DOAs, $F=4$

Fig. 3: SNR performance. Frequencies are (a,c) 100 Hz and (b,d) $\{100, 150, 200, 250\}$ Hz. The number of snapshots is $L=10$. DOAs are at (a,b) $45° + U(-.25°, .25°)$ and (c,d) $[-65, 0, 15]° + U(-.25°, .25°)$ (random uniformly distributed grid offsets).

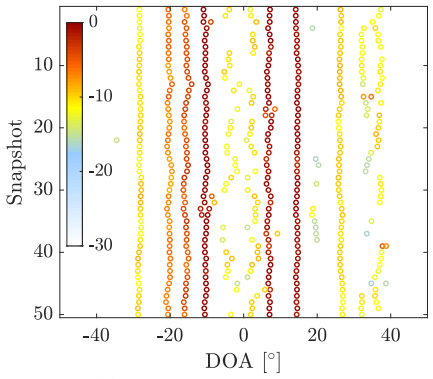

(a) Multi-freq., one snapshot

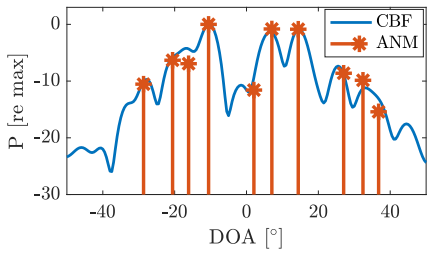

(b) Multi-snapshot-frequency

Fig. 4: DOA estimation using ocean acoustic data from the SWellEx-96 experiment. (a) Single-snapshot multi-frequency AST and (b) Multi-snapshot multi-frequency processing for conventional beamforming (CBF) and AST.

5. SIMULATION AND EXPERIMENTAL RESULTS

We consider a ULA with $M=15$ elements, inter-sensor spacing $d=3$ m, and sound speed $c=1500$ m/s. Frequencies are 100 Hz ($F=1$) and $\{100, 150, 200, 250\}$ Hz ($F=4$). The wavelengths are $\{15, 10, 7.5, 6\}$ m, i.e., d/λ are $\{5, 10/3, 2.5, 2\}$. We compare the DOA estimates produced by our approach to those obtained using SBL [31] using the root-mean-squared error (RMSE):

$$\text{RMSE} = \sqrt{\mathbb{E}\left[\frac{1}{K}\sum_{k=1}^{K}\left(\hat{\theta}_k - \theta_k^{\text{true}}\right)^2\right]}. \tag{18}$$

The angular search grid is discretized as $[-90:.5:90]°$ for SBL. We use $\tau=.001$ (6) for ANM.

Figure 3 presents four DOA scenarios: (a) a single frequency $F=1$ and (b) multiple frequencies $F=4$ with one DOA at $45° + U(-.25°, .25°)$ and (c) $F=1$ and (d) $F=4$ with three DOAs at $[-65, 0, 15]° + U(-.25°, .25°)$ having a random uniformly distributed grid mismatch. Each RMSE is averaged over 100 trials. The sources have equal amplitudes, each with random phases on $[0, 2\pi)$ at SNRs $[-20:5:30]$ dB. The superior performance of ANM in the high SNR region is illustrated by the curve lying on the Cramér-Rao bound (CRB) [32, Eq. (110)]. SBL exhibits bias even at high SNRs due to grid mismatch. To achieve CRB-like performance, a grid spacing of at least $0.01°$-interval was required.

We validate the proposed method using ocean acoustic data from the SWellEx-96 experiment [13, 31, 33]. The data used is the first 50 snapshots in [13] with $F=2$, $\{f_1, f_2\} = \{112, 166\}$ Hz, i.e., $f_2 = 1.48 f_1 \approx 1.5 f_1$ gives $f_{\mathcal{N}} = f_1/2$ and $N=3$. We used elements 1–60 in the ULA ($M=60$).

The dataset includes multiple stationary DOAs across time, suitable for multi-snapshot processing, see Fig. 4. We have chosen $K=10$ strongest DOA estimates. For the associated arrival paths with the estimated DOAs, see [13].

Single-snapshot processing with the proposed multi-frequency ANM obtains good DOA estimates. Multi-snapshot processing also achieves DOA estimates consistent across multiple snapshots. The proposed method achieves processing gain for accurate estimates by considering multiple measurement vectors (multi-snapshot and multi-frequency) compared to the single-snapshot single-frequency model.

6. CONCLUSION

A DOA estimation algorithm is developed for multiple data across time and frequency. Multi-snapshot-frequency processing employs the nominal frequency-virtual array element spacing, allowing alignment of multi-frequency samples with multi-snapshot samples, thus addressing both time and frequency simultaneously. Incorporating more frequencies and snapshots enhances the DOA performance, as demonstrated by its effectiveness on real data.

7. REFERENCES

[1] G. Tang, B. N. Bhaskar, P. Shah, and B. Recht, "Compressed sensing off the grid," *IEEE Trans. Inf. Theory*, vol. 59, no. 11, pp. 7465–7490, Nov. 2013.

[2] E.J. Candès and C. Fernandez-Granda, "Towards a mathematical theory of super-resolution," *Commun. Pure Appl. Math.*, vol. 67, no. 6, pp. 906–956, Apr. 2014.

[3] Z. Yang and L. Xie, "On gridless sparse methods for line spectral estimation from complete and incomplete data," *IEEE Trans. Signal Process.*, vol. 63, no. 12, pp. 3139–3153, Jun. 2015.

[4] S. Li, D. Yang, G. Tang, and M. B. Wakin, "Atomic norm minimization for modal analysis from random and compressed samples," *IEEE Trans. Signal Process.*, vol. 66, no. 7, pp. 1817–1831, Jan. 2018.

[5] S. Li, M. B. Wakin, and G. Tang, "Atomic norm denoising for complex exponentials with unknown waveform modulations," *IEEE Trans. Inf. Theory*, vol. 66, no. 6, pp. 3893–3913, Nov. 2019.

[6] Y. Chi and M. Ferreira Da Costa, "Harnessing sparsity over the continuum: Atomic norm minimization for superresolution," *IEEE Signal Process. Mag.*, vol. 37, no. 2, pp. 39–57, Mar. 2020.

[7] H. Groll, P. Gerstoft, M. Hofer, J. Blumenstein, T. Zemen, and C. F. Mecklenbräuker, "Scatterer identification by atomic norm minimization in vehicular mm-Wave propagation channels," *IEEE Access*, vol. 10, pp. 102334–102354, Sep. 2022.

[8] M. Pesavento, M. Trinh-Hoang, and M. Viberg, "Three more decades in array signal processing research: An optimization and structure exploitation perspective," *IEEE Signal Process. Mag.*, vol. 40, no. 4, pp. 92–106, Jun. 2023.

[9] Z. Yang, J. Li, P. Stoica, and L. Xie, "Sparse methods for direction-of-arrival estimation," in *Academic Press Library in Signal Processing: Array, Radar and Communications Engineering*, vol. 7, chapter 11, pp. 509–581. Academic Press, 2018.

[10] A. Xenaki and P. Gerstoft, "Grid-free compressive beamforming," *J. Acoust. Soc. Am.*, vol. 137, no. 4, pp. 1923–1935, Apr. 2015.

[11] Y. Park, Y. Choo, and W. Seong, "Multiple snapshot grid free compressive beamforming," *J. Acoust. Soc. Am.*, vol. 143, no. 6, pp. 3849–3859, Jun. 2018.

[12] M. Wagner, Y. Park, and P. Gerstoft, "Gridless DOA estimation and root-MUSIC for non-uniform linear arrays," *IEEE Trans. Signal Process.*, vol. 69, pp. 2144–2157, Mar. 2021.

[13] Y. Park and P. Gerstoft, "Gridless sparse covariance-based beamforming via alternating projections including co-prime arrays," *J. Acoust. Soc. Am.*, vol. 151, no. 6, pp. 3828–3837, Jun. 2022.

[14] D. Malioutov, M. Cetin, and A. S. Willsky, "A sparse signal reconstruction perspective for source localization with sensor arrays," *IEEE Trans. Signal Process.*, vol. 53, no. 8, pp. 3010–3022, Aug. 2005.

[15] A. Xenaki, P. Gerstoft, and K. Mosegaard, "Compressive beamforming," *J. Acoust. Soc. Am.*, vol. 136, no. 1, pp. 260–271, Jul. 2014.

[16] P. Gerstoft, A. Xenaki, and C. F. Mecklenbräuker, "Multiple and single snapshot compressive beamforming," *J. Acoust. Soc. Am.*, vol. 138, no. 4, pp. 2003–2014, Oct. 2015.

[17] Y. Chi, L. L. Scharf, A. Pezeshki, and A. R. Calderbank, "Sensitivity to basis mismatch in compressed sensing," *IEEE Trans. Signal Process.*, vol. 59, no. 5, pp. 2182–2195, May 2011.

[18] C. Fernandez-Granda, "Super-resolution of point sources via convex programming," *Inf. Inference*, vol. 5, no. 3, pp. 251–303, Apr. 2016.

[19] Y. Chi and Y. Li, "Off-the-grid line spectrum denoising and estimation with multiple measurement vectors," *IEEE Trans. Signal Process.*, vol. 64, no. 5, pp. 1257–1269, Oct. 2016.

[20] P. Chen, Z. Chen, Z. Cao, and X. Wang, "A new atomic norm for DOA estimation with gain-phase errors," *IEEE Trans. Signal Process.*, vol. 68, pp. 4293–4306, Jul. 2020.

[21] S. Qin, Y. D. Zhang, M. G. Amin, and B. Himed, "DOA estimation exploiting a uniform linear array with multiple co-prime frequencies," *Signal Process.*, vol. 130, pp. 37–46, Jan. 2017.

[22] F. Wang, Z. Tian, G. Leus, and J. Fang, "Direction of arrival estimation of wideband sources using sparse linear arrays," *IEEE Trans. Signal Process.*, vol. 69, pp. 4444–4457, Jul. 2021.

[23] S. Zhang, A. Ahmed, Y. D. Zhang, and S. Sun, "Enhanced DOA estimation exploiting multi-frequency sparse array," *IEEE Trans. Signal Process.*, vol. 69, pp. 5935–5946, Oct. 2021.

[24] Y. Wu, M. B. Wakin, and P. Gerstoft, "Gridless DOA estimation under the multi-frequency model," in *Proc. IEEE ICASSP*, 2022, pp. 5982–5986.

[25] Y. Wu, M. B. Wakin, and P. Gerstoft, "Gridless DOA estimation with multiple frequencies," *IEEE Trans. Signal Process.*, vol. 71, pp. 417–432, Feb. 2023.

[26] Y. D. Zhang and M. G. Amin, "Multi-frequency rational sparse array for direction-of-arrival estimation," in *Proc. IEEE ISSCS*, 2023, pp. 1–4.

[27] Y. Wu, M. B. Wakin, and P. Gerstoft, "Non-uniform array and frequency spacing for regularization-free gridless DOA," *IEEE Trans. Signal Process.*, vol. 72, pp. 2006–2020, Apr. 2024.

[28] B. N. Bhaskar, G. Tang, and B. Recht, "Atomic norm denoising with applications to line spectral estimation," *IEEE Trans. Signal Process.*, vol. 61, no. 23, pp. 5987–5999, Dec. 2013.

[29] C. Steffens, M. Pesavento, and M. E. Pfetsch, "A compact formulation for the $\ell_{2,1}$ mixed-norm minimization problem," *IEEE Trans. Signal Process.*, vol. 66, no. 6, pp. 1483–1497, Mar. 2018.

[30] M. Grant and S. Boyd, "CVX: Matlab software for disciplined convex programming, version 2.2," 2014, (Last viewed June 20, 2023).

[31] S. Nannuru, K. L. Gemba, P. Gerstoft, W. S. Hodgkiss, and C. F. Mecklenbräuker, "Sparse Bayesian learning with multiple dictionaries," *Signal Process.*, vol. 159, pp. 159–170, Feb. 2019.

[32] H. L. Van Trees, *Optimum Array Processing (Detection, Estimation, and Modulation Theory, Part IV)*, John Wiley & Sons, New York, 2002.

[33] K. L. Gemba, S. Nannuru, and P. Gerstoft, "Robust ocean acoustic localization with sparse Bayesian learning," *IEEE J. Sel. Topics Signal Process.*, vol. 13, no. 1, pp. 49–60, Mar. 2019.